

Hybrid Residual Correction of VMC Charmonium Masses with a Screened Funnel Interaction

Tarik Akan^{1*}, Metin Yalvac^{2†}

^{1,2}Physics Department, Yozgat Bozok University, 66100 Yozgat, Turkey

July 3, 2026

Abstract

In this study, we combine residual correction with the physical treatment of charmonium masses within a Quantum Chromodynamics (QCD) motivated potential-model framework via variational Monte Carlo (VMC). The aim is not to propose a new charmonium spectrum, since this sector has already been examined extensively through different potential models. Instead, the main objective is to evaluate how effectively a Machine Learning (ML) correction can improve a VMC baseline when both stages are built on the same screened funnel potential. In this workflow, the screened interaction provides the physical input and determines the underlying mass structure. The proposed run uses the variational method via VMC and deterministic eigenvalue diagonalization in the process of mass calculation. In total, ten charmonium states are calculated, among which seven use the experimental reference masses. The VMC step generates a large set of configurations and local energy estimators that are fed into the neural network (NN) residual corrector at the sample level, while the corrections and experimental uncertainties are collected at the state level. It then learns the residual difference between the raw physics baseline and the internal reference targets. This hybrid procedure reduces the systematic mass offset of the raw calculation across the studied states. For the experimentally verified seven states, the correction reduces the MAE from 438.1 MeV to 24.1 MeV, corresponding to a 94.5% reduction. These results show that ML can serve as a residual-correction layer for potential-model spectroscopy.

1 Introduction

Charmonium remains a crucial test case for models of heavy-quark dynamics. Its spectrum is experimentally constrained by the Particle Data Group (PDG) compilations, which provide stable reference masses for numerical validation [1–3]. The system also lies in an energy regime where nonrelativistic intuition remains useful. This feature explains the long-standing role of potential models in charmonium spectroscopy [4, 5]. The Cornell interaction established a useful balance between short-range Coulomb attraction and long-range confinement [4, 5]. Later relativized approaches extended this framework by including spin-dependent and kinematic effects [6]. Many studies have refined heavy-quark spectra through modified potentials, improved parameter searches, and alternative solvers. Flavor-wide spectroscopy constrains heavy-quark interactions across charm and beauty sectors [7]. Excited charmonium states provide an additional test of these interactions because their masses are sensitive to model details [8]. Electromagnetic transitions offer another constraint, since higher multipole effects probe the same wave functions [9]. Recent studies have extended this program with Cornell-type, exponential, quadratic, mixed, and screened potentials [10–14]. These works show that potential choice and parameterization strongly affect predicted masses. They also indicate that another isolated mass fit has limited novelty. The more relevant issue is computational. In the present work, we use a screened funnel potential that retains the short-distance Coulomb attraction while replacing the un-screened linear confinement with a softened long-distance contribution. Even with such a physical baseline, systematic residual structure may remain. An ML layer can model this residual structure

*tarik.akan@bozok.edu.tr (Corresponding author)

†metin.yalvac@bozok.edu.tr

when the baseline preserves the relevant spectral ordering. For this reason, ML is treated here as a correction to VMC, not as a replacement for the physical model.

The screened funnel potential is well suited to this purpose because it modifies the confining interaction at large separation. Color screening has a direct QCD motivation in studies of heavy-quark bound states at finite temperature and in medium [15, 16]. It is also relevant for excited levels, which probe larger distances than low-lying states [8, 9]. A screened interaction therefore provides a demanding baseline for residual learning. It contains enough physical structure to encode short-distance attraction and confinement, while still allowing systematic numerical deviations to remain. Cornell-based studies already show that the parameter space of heavy-quark potentials is nontrivial [10, 17]. The present work follows this logic with a different emphasis. We optimize the screened funnel parameters for mass resolution within the adopted model and then examine how much of the remaining discrepancy can be recovered through ML residual correction.

VMC provides a natural physics baseline because it evaluates quantum expectation values through stochastic sampling. Monte Carlo methods have long been used in nonrelativistic QCD and heavy-hadron calculations [18, 19]. Stochastic reconfiguration also illustrates how Monte Carlo optimization can improve quantum variational calculations [20]. These approaches are valuable because they preserve a direct connection between wave functions, Hamiltonians, and observables. At the same time, incomplete trial spaces, imperfect parameter choices, or limitations of the potential form can generate structured residual errors. Such errors are not merely random fluctuations. They may contain learnable information about missing corrections or solver bias. This makes them suitable targets for supervised ML. ML is trained to correct the remaining mass residuals.

ML has become an important practical tool for representation and optimization in quantum many-body physics. NN wave functions, for example, have shown that artificial neural networks can solve quantum many-body problems through flexible variational forms [21]. In hadron spectroscopy, neural approaches have also been used with Cornell and mixed heavy-quark potentials [13, 22]. These studies support the use of learning methods for nonlinear spectral corrections. Our contribution, however, has a more restricted role. We do not use ML to replace the potential model. Instead, it is applied after the screened funnel VMC calculation, so that the physical ordering imposed by the Hamiltonian is preserved and the learning task is limited to the residual structure.

The broader aim of this work is methodological. Charmonium spectroscopy already has a rich set of potential-model analyses [4, 6, 8, 12] and precise experimental anchors for testing numerical predictions [1]. This combination makes it a suitable laboratory for hybrid physics–ML workflows. In our approach, the screened funnel potential supplies the dynamical baseline, VMC provides the stochastic quantum solver, and ML supplies the residual map from baseline masses to corrected masses. The paper evaluates this workflow rather than proposing a new charmonium catalogue. The success of the method is measured by the improvement over the same VMC baseline, not by claiming that the screened funnel potential is a definitive description of charmonium. A technical issue is also important in order to understand the ML phase. In the run under investigation, there are ten charmonium states, of which seven states use the experimental reference masses and are used in the residual analysis. However, the ML data set is not limited only to seven points. For each member of charmonium spectroscopy, the VMC method produces a large set of radial wave functions, local energies, potential values, and variational parameters. These VMC-generated values are included in the regression process, and then the results at the sample level are averaged in order to produce one corrected mass for each state. The following sections define the screened funnel model, describe the VMC and ML procedure, and quantify the residual correction across the selected states.

2 Methodology

We formulate charmonium as a nonrelativistic two-body $c\bar{c}$ system. This choice follows the potential-model tradition for heavy quarkonia [4–6]. We therefore use the potential model as a controlled physics input.

$$H\psi_{nlm}(\mathbf{r}) = E_{nl}\psi_{nlm}(\mathbf{r}), \quad (1)$$

where H is the relative Hamiltonian, ψ_{nlm} is the charmonium wave function, and E_{nl} is the binding energy. The quantum numbers n , l , and m denote the radial, orbital, and magnetic labels. The reduced mass is defined as

$$\bar{m} = \frac{m_c}{2}, \quad (2)$$

since $m_c = m_{\bar{c}}$ for charmonium. The Hamiltonian is

$$H = -\frac{1}{2\bar{m}}\nabla^2 + V(r), \quad (3)$$

where $r = |\mathbf{r}|$ is the quark–antiquark separation. This form isolates the central interaction. It also gives a transparent baseline for testing ML residual learning.

The interaction is taken as a screened funnel potential. It combines short-distance Coulomb attraction with a screened confining term. This structure reflects the physical role of color Coulomb exchange and confinement in quarkonium models [4, 5]. Screening is included because heavy-quark bound states can feel medium-like or channel-induced flattening effects at larger distance [15, 16]. The potential is written as

$$V(r) = -\frac{\kappa}{r} + \frac{\sigma}{\mu_s} (1 - e^{-\mu_s r}) + V_0, \quad (4)$$

where κ controls the Coulomb strength, σ is the string-tension scale, μ_s is the screening parameter, and V_0 is a constant shift. For the analyzed run, the recorded inputs are $m_c = 1.27$ GeV, $\sigma = 0.273073$ GeV², $\kappa = 0.699732$, $V_0 = -0.322296$ GeV, and $\mu_s = 0.128287$ GeV. In the limit $\mu_s r \ll 1$, the confining part becomes approximately linear. This connects the model to Cornell-type spectroscopy [4, 10, 17]. The expansion is

$$\frac{\sigma}{\mu_s} (1 - e^{-\mu_s r}) = \sigma r - \frac{\sigma\mu_s}{2}r^2 + \mathcal{O}(r^3), \quad (5)$$

here the first term gives the usual linear confinement. At large r , the same term saturates. This saturation gives a direct mathematical representation of screening.

The radial wave function is separated as

$$\psi_{nlm}(\mathbf{r}) = \frac{u_{nl}(r)}{r} Y_{lm}(\theta, \phi), \quad (6)$$

where Y_{lm} is the spherical harmonic. The radial equation becomes

$$\left[-\frac{1}{2\bar{m}} \frac{d^2}{dr^2} + \frac{l(l+1)}{2\bar{m}r^2} + V(r) \right] u_{nl}(r) = E_{nl} u_{nl}(r), \quad (7)$$

where $l(l+1)/(2\bar{m}r^2)$ is the centrifugal term. This equation defines the VMC target. Similar radial reductions are standard in quark–antiquark spectral calculations [23, 24]. We use them here only to define the numerical estimator.

The physical mass of a spin-averaged state is computed as

$$M_{nl}^{\text{VMC}} = 2m_c + E_{nl}, \quad (8)$$

M_{nl}^{VMC} is the raw VMC mass. The term “VMC baseline” refers to the physical baseline with VMC on. The masses that appear in the table are the results of eigensolver computations and are not averages obtained directly from the Monte Carlo sampling. The spin-dependent splitting is not fitted separately in this case. Higher charmonium calculations often include richer spin and transition structures [8, 9, 12]. The present design instead tests whether ML can correct systematic VMC bias within one fixed baseline.

The VMC calculation uses a trial wave function with explicit n and l dependence. We choose a radial form that enforces regularity at the origin. It also provides exponential decay at large distance. The trial state is

$$u_{nl}^T(r; \boldsymbol{\alpha}) = \mathcal{N}_{nl} r^{l+1} P_n(r; \boldsymbol{\alpha}) e^{-\alpha r - \beta r^2}, \quad (9)$$

where \mathcal{N}_{nl} normalizes the state. The vector $\boldsymbol{\alpha}$ contains the variational parameters. The parameters α and β control the radial falloff. The polynomial P_n supplies radial structure. This ansatz gives sufficient flexibility for low charmonium levels. It also preserves a compact parameter space for stable VMC optimization. For excited states, the polynomial factor $P_n(r; \alpha)$ is used to encode the radial-node structure associated with the chosen (n, l) channel. Thus, each state is treated with a state-specific trial function rather than by reusing the same radial profile for all levels. The variational parameters are optimized separately for every (n, l) channel, while the imposed radial form fixes the required near-origin behavior through r^{l+1} and allows the excited-state structure through P_n . This construction prevents the excited-state calculation from being interpreted as a simple repetition of the ground-state VMC run. In this work, the VMC energies for the excited channels are therefore obtained from independently optimized trial states carrying the corresponding radial and orbital labels.

The probability density sampled in VMC is

$$\rho_{nl}(r; \boldsymbol{\alpha}) = \frac{|u_{nl}^T(r; \boldsymbol{\alpha})|^2}{\int_0^\infty |u_{nl}^T(r; \boldsymbol{\alpha})|^2 dr}, \quad (10)$$

where the denominator enforces normalization. The local energy is

$$E_L(r; \boldsymbol{\alpha}) = \frac{H u_{nl}^T(r; \boldsymbol{\alpha})}{u_{nl}^T(r; \boldsymbol{\alpha})}, \quad (11)$$

measures the pointwise action of the Hamiltonian. The variational energy is then

$$E_{nl}^T(\boldsymbol{\alpha}) = \int_0^\infty \rho_{nl}(r; \boldsymbol{\alpha}) E_L(r; \boldsymbol{\alpha}) dr, \quad (12)$$

and the Monte Carlo estimator is

$$\widehat{E}_{nl}^T(\boldsymbol{\alpha}) = \frac{1}{N_s} \sum_{i=1}^{N_s} E_L(r_i; \boldsymbol{\alpha}), \quad (13)$$

where N_s is the number of sampled radial points. The points r_i are distributed according to ρ_{nl} . This estimator is the numerical core of the VMC baseline. The sampled configuration along with its energy and potentials, which were produced through Monte Carlo sampling process for each experimental ground state charmonium, are kept as a training instance in ML algorithm, and hence the dataset is made up of the VMC generated samples rather than seven ground state masses. The mass value of an experimental ground state is still the common physical anchor point for those samples corresponding to that state.

The variational parameters minimize the estimated energy. The optimization problem is handled by

$$\boldsymbol{\alpha}_{nl}^* = \arg \min_{\boldsymbol{\alpha}} \widehat{E}_{nl}^T(\boldsymbol{\alpha}), \quad (14)$$

with $\boldsymbol{\alpha}_{nl}^*$ optimized parameters for each state. This variational principle connects the method to standard stochastic wave-function optimization. Stochastic reconfiguration and related Monte Carlo methods show how correlated sampling can stabilize quantum variational calculations [20]. Our implementation uses the same principle of energy minimization. It keeps the numerical objective explicit and reproducible. In this way, the screened funnel parameters are optimized at the spectrum level. We define a parameter vector

$$\boldsymbol{\theta} = (m_c, \kappa, \sigma, \mu_s, V_0), \quad (15)$$

here each component has a direct physical role. The spectrum-level loss is

$$\mathcal{L}_{\text{VMC}}(\boldsymbol{\theta}) = \frac{1}{N_{\mathcal{A}}} \sum_{j \in \mathcal{A}} \left(M_j^{\text{VMC}}(\boldsymbol{\theta}) - M_j^{\text{ref}} \right)^2, \quad (16)$$

where \mathcal{A} denotes the experimentally anchored state set and $N_{\mathcal{A}} = 7$ for the analyzed run. Ten channels are computed in total, while the seven states provide the reference targets used for parameter

calibration and residual learning. The reference values M_j^{ref} are the state-level target masses. The loss does not serve as a discovery criterion. It defines the best numerical resolution of the adopted screened potential.

Neural quantum-state methods show that ML can represent complex many-body structure [21]. Neural-network studies of Cornell-type systems also motivate ML as a numerical surrogate for potential-model errors [13, 22]. The network does not replace the Hamiltonian. It learns the remaining mass error after VMC.

For each experimentally verified state j , the state-level residual target is

$$\Delta_j = M_j^{\text{ref}} - M_j^{\text{base}}, \quad M_j^{\text{base}} \equiv M_j^{\text{VMC}}, \quad (17)$$

where M_j^{base} denotes the VMC-enabled eigensolver baseline. Although Δ_j is anchored by the reference mass of state j , it is learned from the VMC sample ensemble generated for that state. For sampled configuration i in state j , the ML input can be represented as

$$x_{ij} = (r_{ij}, E_L(r_{ij}), V(r_{ij}), n_j, l_j, M_j^{\text{base}}, m_c, \kappa, \sigma, \mu_s, V_0, \phi_{ij}), \quad (18)$$

where ϕ_{ij} denotes any additional sample-level or variational descriptors retained by the numerical run. The network predicts a sample-level residual response,

$$\hat{\Delta}_{ij} = f_w(x_{ij}), \quad (19)$$

and the correction assigned to state j is obtained by aggregating its $N_{s,j}$ VMC samples,

$$\hat{\Delta}_j = \frac{1}{N_{s,j}} \sum_{i=1}^{N_{s,j}} \hat{\Delta}_{ij}. \quad (20)$$

The corrected state mass is therefore

$$M_j^{\text{ML}} = M_j^{\text{base}} + \hat{\Delta}_j. \quad (21)$$

The ML objective is defined over all VMC-generated samples belonging to the anchored state set \mathcal{A} ,

$$L_{\text{ML}}(w) = \frac{1}{N_{\text{ML}}} \sum_{j \in \mathcal{A}} \sum_{i=1}^{N_{s,j}} [\Delta_j - f_w(x_{ij})]^2 + \eta \|w\|_2^2, \quad N_{\text{ML}} = \sum_{j \in \mathcal{A}} N_{s,j}. \quad (22)$$

Thus, N_{ML} represents the total number of VMC training samples, which is very large compared to experimental references. In that stage, VMC ensembles provide the variation at the level of the sample necessary for the regression. Since all samples from the same state have a common target to refer to, they may be statistically correlated. Hence, the large number of samples, cannot be considered as seven independent measurements of the experiment.

As a summary of methodology, the workflow therefore has three linked stages. First, the screened funnel Hamiltonian creates a physical motivation for the baseline. Next, the optimization and deterministic eigensolver using the VMC allows the baseline masses to be obtained. Finally, machine learning learns the residual error on the sample ensembles created using the VMC with the seven state level references as targets. This is a controlled way of obtaining the final result. The final result masses are not derived from an unconstrained black box. At the end, we evaluate the residual correction with compact global metrics, such as MAE, RMSE, and R^2 . Basically, they measure the numerical success of the residual correction.

3 Results and Discussion

The numerical results are evaluated as a residual-correction problem applied to the VMC mass baseline. provides the physics baseline. The ML model then learns the residual between this baseline and

the reference charmonium masses. This design keeps the potential model in the calculation. It also prevents the ML layer from replacing the Schrödinger dynamics with a purely statistical fit. Such a hybrid strategy matches the present aim: classification of the charmonium spectrum, many interactions and parameter choices [4–6,10]. The present test asks a narrower question. It asks whether ML can remove the systematic residuals that remain after the screened funnel VMC calculation. This question is meaningful because charmonium has precise reference masses in the Particle Data Group tables [1, 2]. It is also meaningful because the screened interaction contains physics beyond the unscreened Cornell form [15–17]. The screened funnel potential controls the baseline before any ML correction is applied. Figure 1 shows the effective running of the string tension in the screened interaction. The figure illustrates why the potential differs from a fixed Cornell confinement term. The confinement strength changes with the interquark distance. This feature is relevant for excited charmonium, where the wave function samples larger distances than the ground state [8,9]. Screening therefore modifies the level spacings before the residual model is trained. On the other hand, Figure 2 shows the change in the potential value at the selected reference radius under parameter perturbations. The dominant entries identify which parameters modify this local potential scale most strongly. This is important for the present argument. The ML correction should improve a tuned physics baseline. It should not compensate for an uncontrolled parameter choice. Similar parameter sensitivity appears in Cornell-type studies, where different parameter regions can reproduce different parts of the heavy-quark spectrum [10, 17]. The screened funnel form therefore supplies a useful but nontrivial baseline for the VMC calculation.

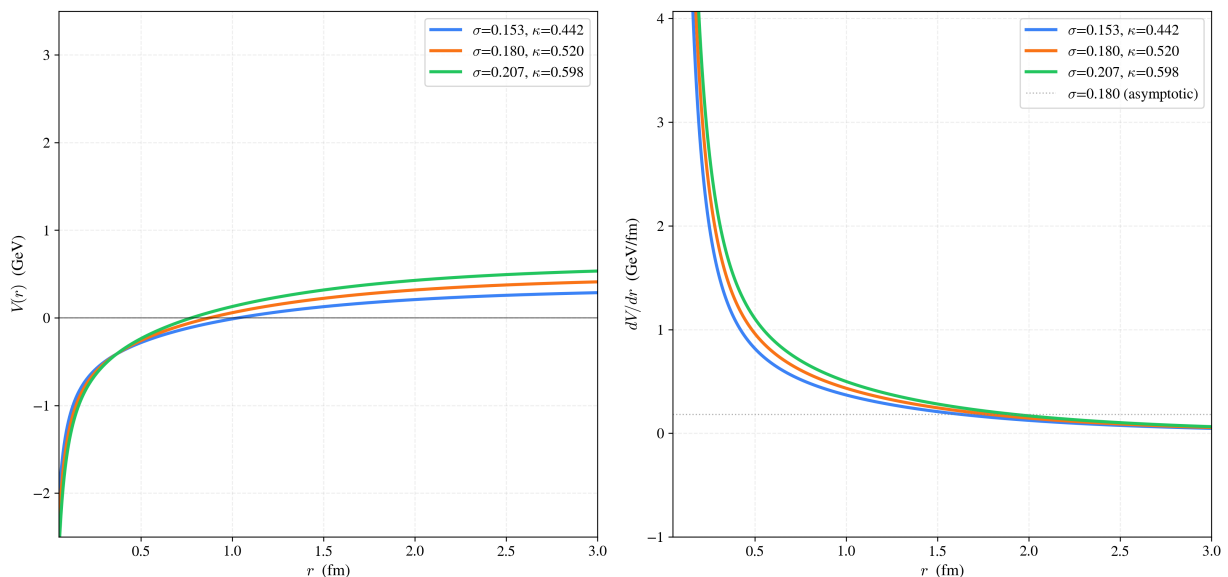


Figure 1: Screened funnel potential and its radial derivative as functions of the interquark separation r . The left panel shows $V(r)$ for different parameter sets (σ, κ) , while the right panel shows dV/dr for the same parameter sets.

The mass and residual comparison is summarized in Fig. 3. for the selected charmonium channels. The lower panel shows the corresponding VMC and ML residuals in MeV. The residual correction procedure is then interpreted as an additive correction to the VMC baseline, where the ML model learns the remaining difference between the VMC prediction and the reference mass. This procedure differs from direct mass prediction. A direct predictor must learn the full spectrum from data. A residual predictor learns the missing correction after the physics solver has already imposed the main structure. This distinction is central to the interpretation of the results. NN methods have been used to approximate spectra in potential models [13,22]. Neural quantum-state methods also show that ML can represent quantum many-body structure in variational settings [21]. The present implementation uses ML in a more constrained role. It corrects the VMC output, while the screened Hamiltonian remains the organizing physical input. The relevant ML hyperparameters define this correction stage. The learning rate controls the update size during training. The number of epochs controls repeated

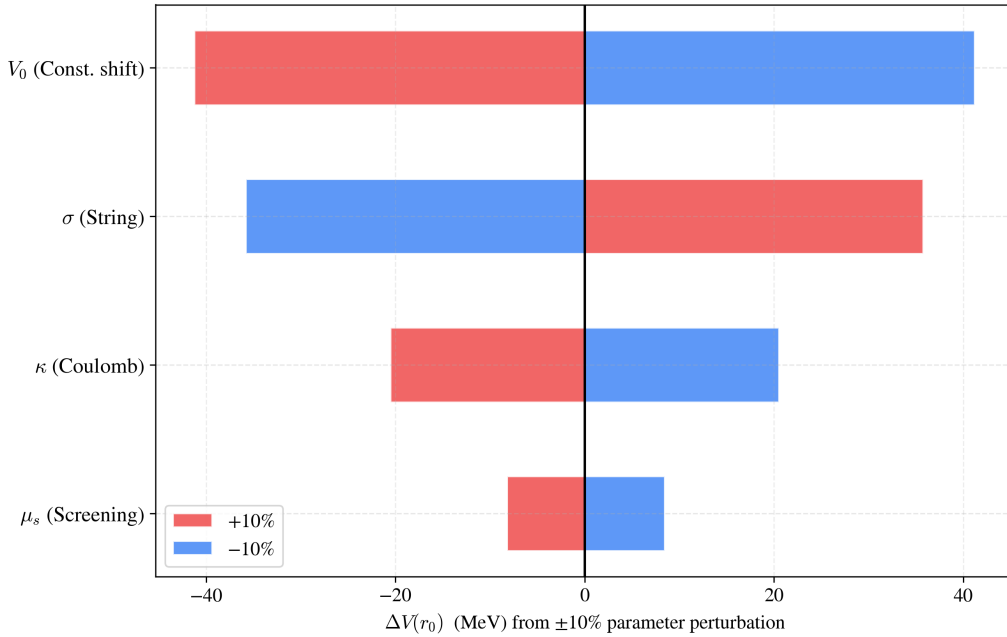


Figure 2: Parameter sensitivity of the screened-funnel baseline. The tornado plot displays the change in the potential at the reference radius, $\Delta V(r_0)$, under $\pm 10\%$ variations of V_0 , σ , κ , and μ_s .

passes through the training set. The hidden layer size defines the expressivity, and the regularization strength constrains overfitting. The train and validation split is done based on the sample dataset created by the VMC for the seven channels that are experimentally defined. It thus relies on numerous sample-based observations rather than seven observations, while the physical performance is assessed afterwards at the level of seven state masses. The correlation of samples within the same VMC ensemble, which have the same state name and reference mass, should also be taken into account when assessing validation scores and generalization to other channels.

For the seven experimentally verified states, the ML correction reduces the raw-baseline MAE from 438.13 MeV to 24.12 MeV, corresponding to a 94.5% improvement. This reduction measures the effect of residual learning at the sample level on the VMC-generated ensembles after they are grouped into seven states. It is not a direct refit of seven isolated mass points. The corrected spectrum gives $\text{RMSE} = 28.77$ MeV, $R^2 = 0.9944$, $\text{MAPE} = 0.66\%$, a maximum absolute error of 48.82 MeV for the $1D$ state, and a mean signed error of -10.53 MeV. The remaining three channels, $2D$, $3P$, and $3D$, are predictions and are excluded from these experimental metrics.

Table 1: The mass comparison for selected charmonium radial-orbital channels.

State	Experimental [1]	ML corrected	Raw baseline	[14]	[8] (NR)	[9] (SP)
1S	3.09693	3.06548	2.5857	2.976	2.982	2.984
1P	3.52538	3.48440	3.0974	-	3.516	3.526
1D	3.77380	3.72498	3.4026	3.705	3.785	3.792
2S	3.68610	3.69072	3.2525	3.550	3.630	3.637
2P	3.92740	3.93339	3.5260	-	3.934	3.916
2D	-	4.08914	3.7259	4.158	4.142	4.095
3S	4.03900	4.05762	3.6346	4.111	4.072	4.030
3P	-	4.24602	3.8170	-	4.279	4.193
3D	-	4.43561	3.9717	-	-	4.336
4S	4.42100	4.43934	3.9039	4.523	4.406	4.281

There are some different spectral notations in the literature. The seven adopted experimental states in the run are $J/\psi(1^3S_1)$ for $1S$, $h_c(1^1P_1)$ for $1P$, $\psi(3770)$ for $1D$, $\psi(2S)$ for $2S$, $\chi_{c2}(3930)$ for $2P$, $\psi(4040)$ for $3S$, and $\psi(4415)$ for $4S$. No experimental value is used for $2D$, $3P$, or $3D$.

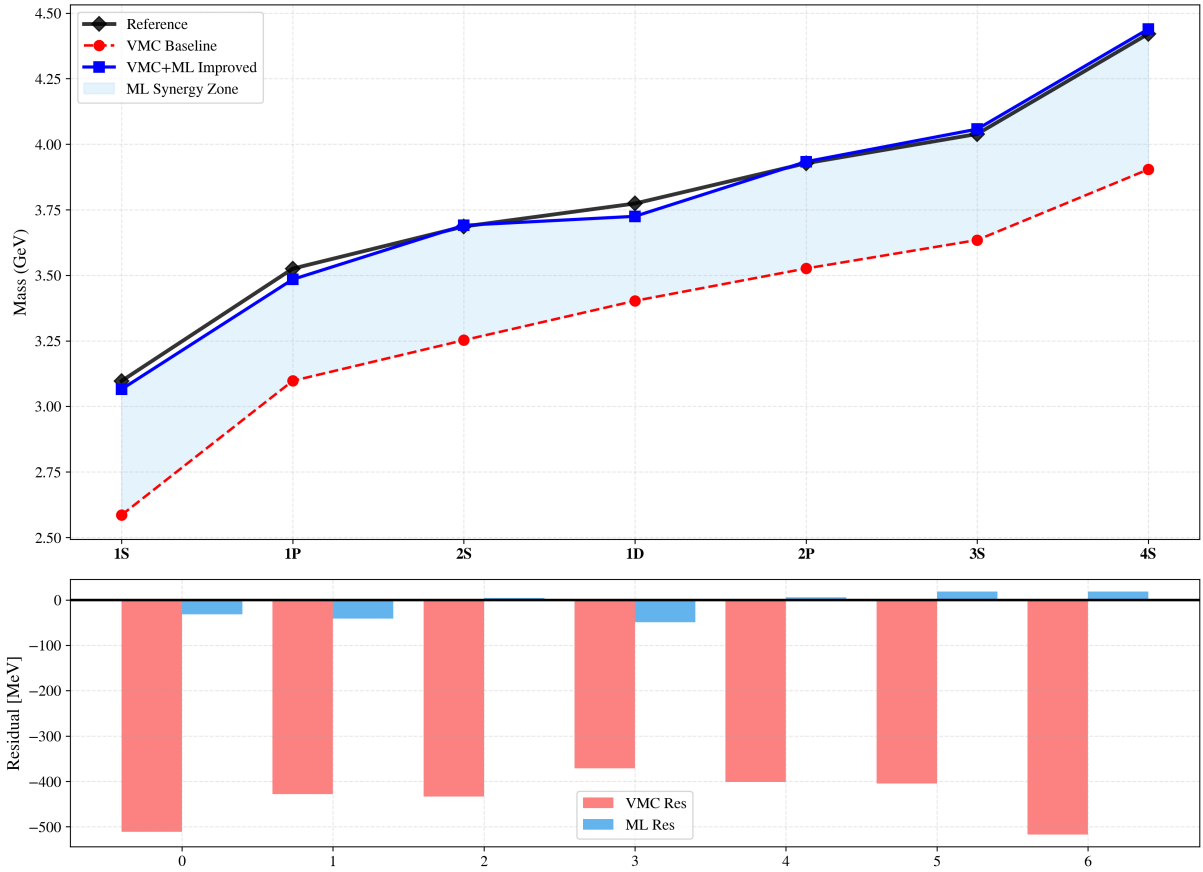


Figure 3: Comparison of the reference targets, raw physics baseline, and ML-corrected charmonium masses. The upper panel shows the seven experimentally anchored states from $1S$ to $4S$, while the lower panel shows the corresponding baseline and corrected residuals in MeV.

Figure 4 illustrates the impact of the training-set size on the residual model. The plotted value is the cross-validation MAE for learning both with and without the physics-prior information. For four included state groups, the curve with the physics prior shows the greater MAE, whereas the curves coincide starting from five to seven groups. However, each data point still consists of the VMC sample ensembles for the included states, so that the horizontal axis reflects the number of spectroscopic groups instead of the number of ML samples. The presented graph does not indicate any obvious advantage of the validation of the prior in this case but provides insight into the effect of introducing additional physical state groups to the regression. This condition is more stringent than the fitting of the training points. It checks whether the model learns the smooth residual pattern among the charmonium states. Figure 5 presents the same result in the target space employed in the analyzed ML run. The corrected masses differ from the adopted references by no more than 49 MeV, while the uncorrected masses exhibit systematic negative deviations by approximately 370–520 MeV. The depicted values correspond to the same seven-state errors used to determine the global metrics provided in Table 1. The model corrects a dominant structured offset rather than small fluctuations. Such residual correction is physically reasonable due to the fact that the potential models usually learn the level ordering better than their absolute locations.

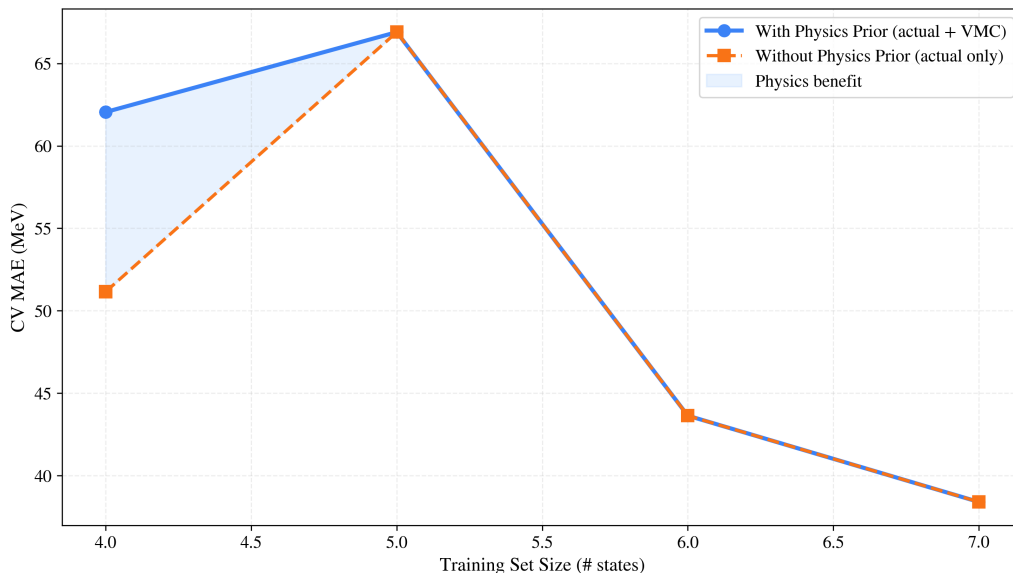


Figure 4: Cross-validation mean absolute error as a function of training-set size. The plot compares residual learning with a physics prior, using actual and VMC-based inputs, against learning without the physics prior, using actual inputs only. The stated training-set size counts included state groups and each group contributes its corresponding VMC sample ensemble.

Moreover, figure 6 adds a more physical view. It compares the splittings between neighboring or related charmonium levels. Mass splittings test the internal structure of the spectrum. They are less sensitive to a common offset than absolute masses. The figure therefore probes whether the ML correction preserves the spectroscopy imposed by the screened VMC baseline. The global ordering is preserved, but the correction does not improve every individual splitting: the $1P \rightarrow 2S$ and $1D \rightarrow 2P$ gaps are overestimated, while the $2S \rightarrow 1D$ gap is underestimated.

MLP gives the smallest test MAE and RMSE, followed by SVR and KNN. RandomForest gives the largest errors in the updated model comparison. These seed-averaged values describe regression over the VMC-generated sample ensembles; they are distinct from the seven aggregated state-mass errors reported in Table 1. Figure 7 compares the test set MAE and RMSE values listed in Table 2 and stands behind the result that the MLP gives the smallest errors, followed by SVR, whereas RandomForest gives the largest values.

Figure 8 places the screened funnel baseline and correction results beside the diagnostic alternatives generated in the current run. For the experimentally verified states, the raw screened-funnel baseline has an MAE of 438.13 MeV and the residually corrected result has an MAE of 24.12 MeV. The

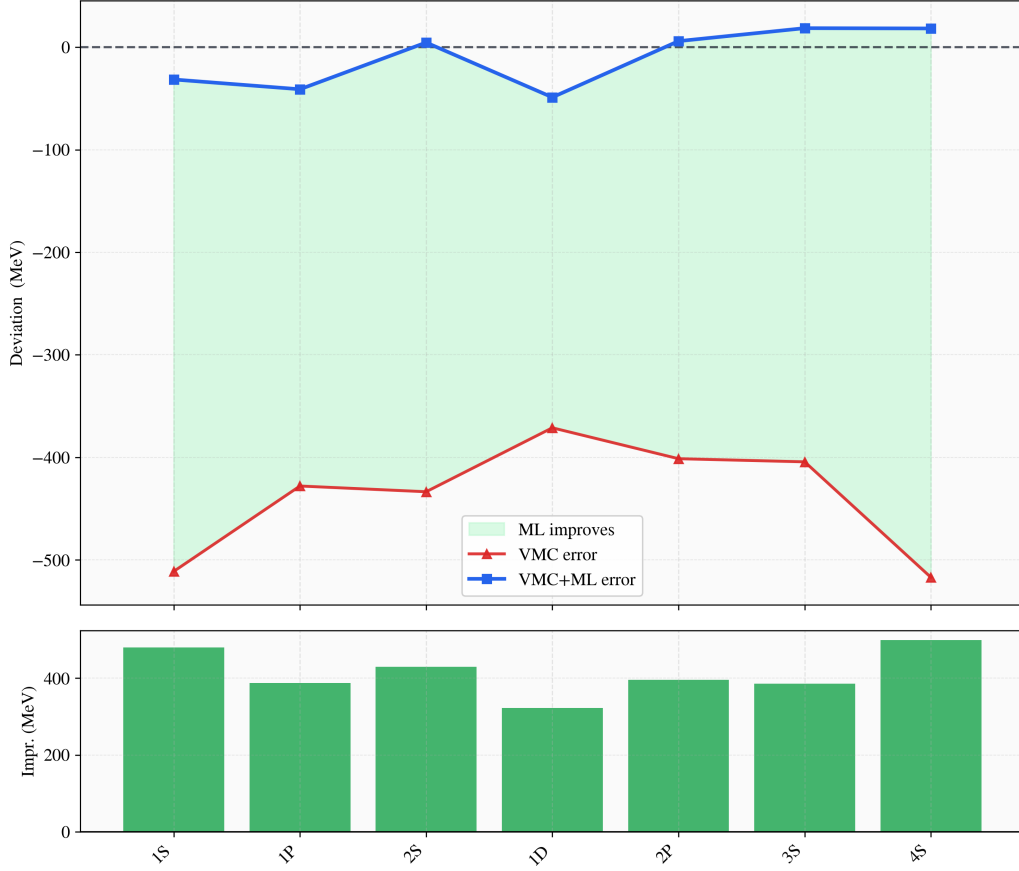


Figure 5: Residual and improvement comparison for the seven experimentally anchored charmonium states. The upper panel shows raw-baseline and ML-corrected deviations from the adopted references, while the lower panel gives the absolute improvement for each state.

Table 2: Test set MAE and RMSE values for the regression models used in the residual-correction stage.

Method	Test MAE (GeV)	Test RMSE (GeV)
ExtraTrees	0.068974 ± 0.000311	0.084481 ± 0.000521
GradientBoosting	0.039944 ± 0.000532	0.048916 ± 0.000716
KNN	0.013841 ± 0.000681	0.018235 ± 0.000894
MLP	0.002334 ± 0.000291	0.003178 ± 0.000351
RandomForest	0.071108 ± 0.000777	0.088543 ± 0.001015
Ridge	0.029055 ± 0.000212	0.039539 ± 0.000153
SVR	0.003961 ± 0.000052	0.004903 ± 0.000044

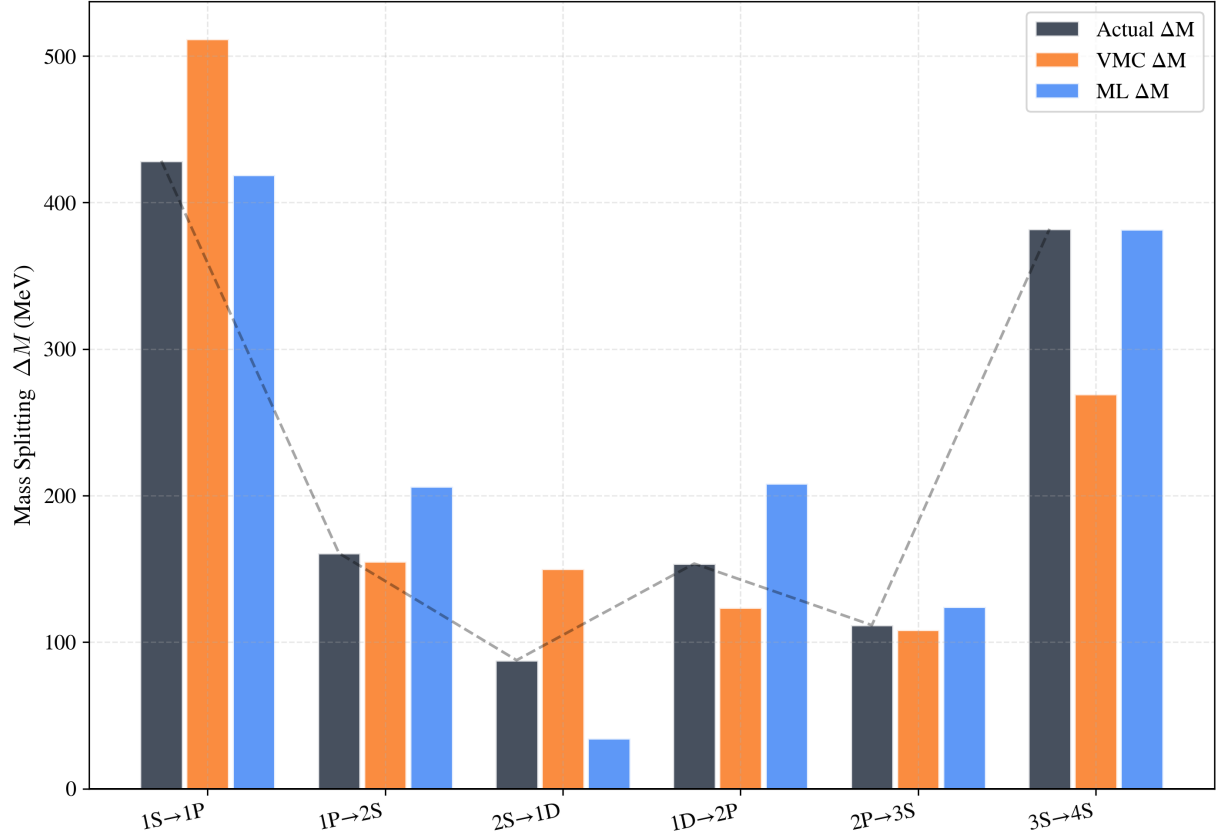


Figure 6: Comparison of charmonium mass splittings for consecutive anchored-state pairs. The grouped bars show the adopted-reference, raw-baseline, and ML-corrected splittings for the transitions from $1S \rightarrow 1P$ through $3S \rightarrow 4S$.

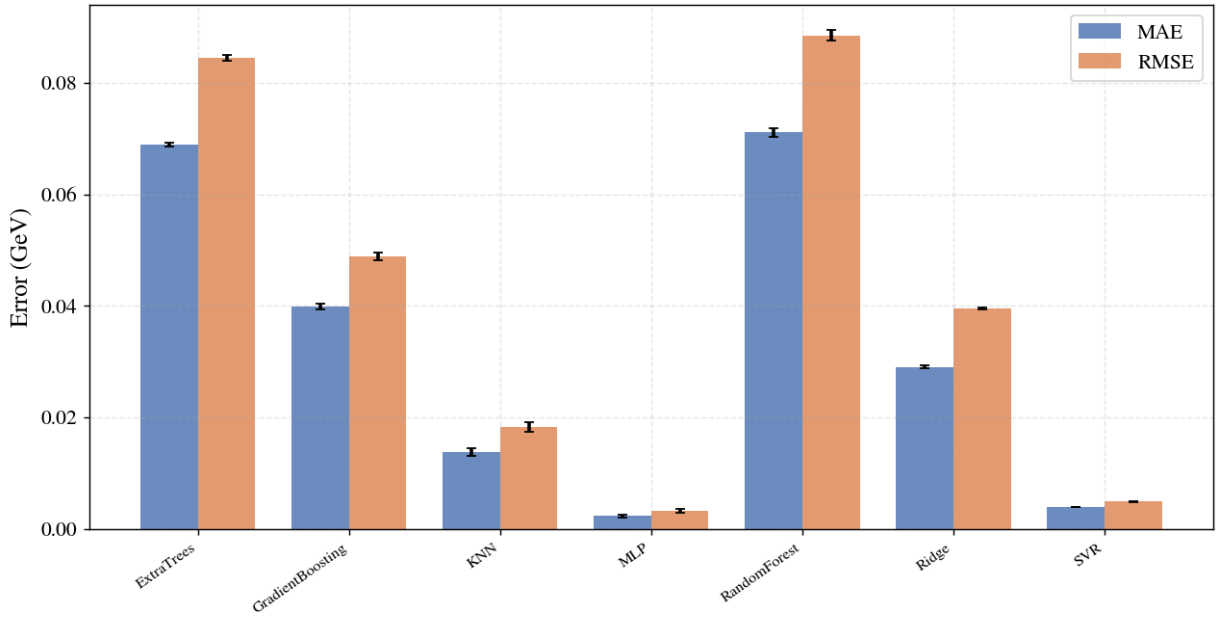


Figure 7: Test-set MAE and RMSE values for the regression models used in the residual-correction stage.

figure also reports 605.30 MeV for the -10% string-tension perturbation, 270.97 MeV for the $+10\%$ perturbation, 298.08 MeV for the mean predictor, and 107.45 MeV for the linear Ridge diagnostic. The comparison is intended to assess the behavior of the present hybrid calculation rather than to establish the universal superiority of a particular potential. Existing Cornell, relativized, exponential, and screened descriptions differ in their treatments of confinement, short-range dynamics, spin effects, and screening [4–6, 11, 12, 14]. The present comparison has a more specific purpose: it shows that the final result should be interpreted as the coupled physics–ML procedure rather than the baseline alone. This result also extends earlier neural-network applications to potential-model spectroscopy [13, 22]. Here, however, the learned correction is applied to the output of the VMC-enabled potential-model workflow. This formulation is compatible with broader stochastic and variational approaches to quantum systems [20, 21].

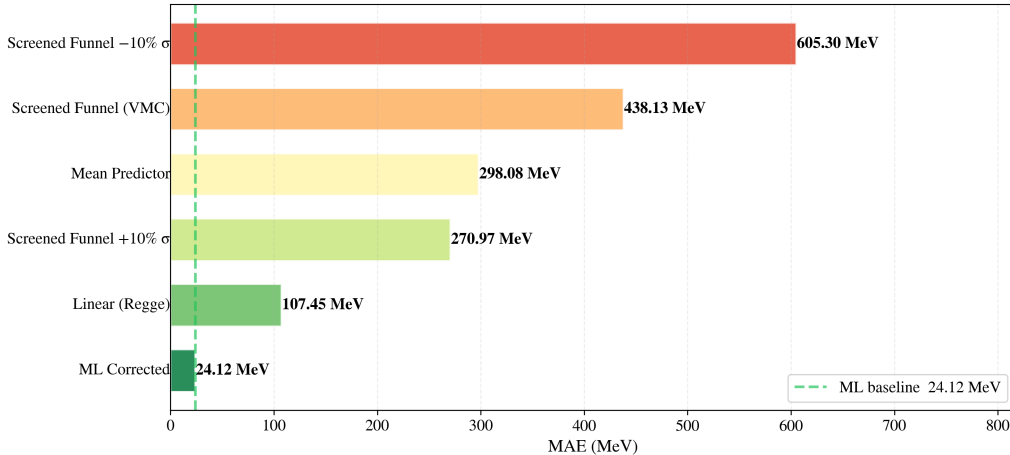


Figure 8: MAE comparison of the baseline and correction diagnostics generated for the current seven-state anchored evaluation. The bars list the mean predictor, $\pm 10\%$ string-tension variations, the raw screened-funnel baseline, the Ridge diagnostic, and the ML-corrected result in MeV.

Placing the present calculation beside earlier charmonium studies helps define its physical scope. Remember that conventional potential models organize the spectrum and provide useful dynamical intuition [6, 7], while screened interactions are particularly relevant for higher states that probe larger interquark separations [15–17]. Recent studies further refine this description through alternative interactions and transition operators [9, 12]. Accordingly, the aim is not to introduce new quantum-number assignments, but to use the established charmonium spectrum as a controlled test of whether residual learning can improve the physics baseline. The learning-curve and mass-splitting diagnostics show that the global offset is strongly reduced and the ordering is retained. The ML training set itself contains many VMC samples for each state, and the main remaining limitation is the finite number of distinct state categories available for testing state-to-state transfer, together with several distorted individual splittings.

The residual model has limits that follow from the data and design. The analyzed ML run contains a large VMC-generated sample ensemble for each of the seven experimentally anchored channels, rather than only seven training observations. This sample-level richness supports nonlinear regression and explains why the MLP can be trained meaningfully. Nevertheless, samples within the same channel share a common physical target and are not equivalent to independent new spectroscopic states. A highly flexible model could exploit within-state redundancy without necessarily transferring to a new radial-orbital channel. Although MLP gives the lowest seed-averaged regression errors in Table 2, transferability to the unobserved $2D$, $3P$, and $3D$ channels should be tested with state-held-out or independently generated ensemble validation. Lower-variance linear or regularized models should therefore remain part of future comparisons.

A more fundamental limitation is the magnitude of the baseline offset. The run uses $m_c = 1.27$ GeV, corresponding to the commonly quoted \overline{MS} charm-mass scale, whereas nonrelativistic potential calculations generally require an effective or pole-like constituent mass. The resulting 438 MeV

baseline MAE and the nearly uniform 400–500 MeV corrections indicate that the neural network is largely learning an additive mass renormalization. The fitted values $\sigma = 0.273073 \text{ GeV}^2$ and $\kappa = 0.699732$ are larger than the values commonly employed in Cornell-type and related charmonium potential models [4–6, 8, 10] and may therefore be compensating for the low mass input. By contrast, the screening parameter $\mu_s = 0.128287 \text{ GeV}$ remains within a physically reasonable range and exhibits weaker local sensitivity. Nevertheless, because all potential parameters are determined simultaneously, μ_s may still be correlated with m_c , V_0 , σ , and κ through the fitting procedure. A physically interpretable follow-up should first repeat the calculation with a pole-like charm mass near 1.5 GeV and then refit all screened-funnel parameters before applying ML.

Still, the corrected output should be interpreted as a sample-level residual-corrected result within the chosen screened funnel potential. It should not be interpreted as an independent solution of QCD. Lattice and effective nonrelativistic QCD calculations address heavy-quark systems from different starting points [18, 19]. Potential models instead provide controlled phenomenological Hamiltonians for spectroscopy [4, 5]. The present contribution belongs to the second category. The methodological contribution is therefore the coupling of the VMC-enabled physics baseline with residual ML correction. Numerically, this coupling lowers the baseline mass error, while physically it retains the spectral organization generated by the screened Hamiltonian.

4 Conclusion

This study examined whether ML residual correction can improve a VMC-enabled eigensolver baseline for the charmonium spectrum obtained with a screened funnel interaction. The potential supplies the short-distance Coulomb attraction and screened long-distance confinement, while the combined variational and diagonalization workflow provides the physical baseline.

The ML stage learns the residual difference between the baseline and the targets from the VMC-generated sample ensembles of the seven experimental values. The training data therefore contain many samples for each state, and the learned responses are aggregated to obtain the final corrected masses. It therefore supplements rather than replaces the Hamiltonian-based calculation. The corrected spectrum retains the level ordering generated by the screened-potential baseline. For the seven experimentally anchored states, the MAE decreases from 438.13 MeV to 24.12 MeV, corresponding to a 94.5% reduction, with RMSE = 28.77 MeV, $R^2 = 0.9944$, and MAPE = 0.66%. The largest remaining deviation is 48.82 MeV for the $1D$ state.

Overall, the results demonstrate that residual learning can reduce systematic mass errors while preserving the main level ordering supplied by the screened funnel potential. Despite this, however, the ML correction itself possesses a considerable, roughly scheme-independent contribution. Such an effect can be, to some extent, explained by the correlations between the chosen value of the charm-quark mass, the shift of the potential due to the constant term, and the rest of the screened funnel parameters. As all the parameters used here have been determined within the same framework, they are to be treated as effective parameters of the current approach, rather than a scheme-independent determination. The focus of the current investigation is the enhancement of the prediction obtained from the combination of the VMC data with ML. The remaining deviations in several excited channels indicate that the method should be interpreted as a VMC-based residual improvement of the potential model rather than an independent solution of QCD. The same workflow can be extended to other heavy-quark systems in which a physically motivated result exhibits structured numerical residuals. The remaining deviations in several excited channels indicate that the method should be interpreted as a VMC-based residual improvement of the potential model rather than an independent solution of QCD. The same workflow can be extended to other heavy-quark systems in which a physically motivated baseline exhibits structured numerical residuals [18, 19, 25, 26].

Acknowledgements

This research was supported by the Scientific Research Projects Coordination Unit of Yozgat Bozok University (BAP) under Project No. FBG-2025-1799. The authors also acknowledge YEKUT, the High

Energy and Quantum Computations Laboratory at Yozgat Bozok University, where the computational part of this study was carried out.

References

- [1] Sea Navas, C Amsler, T Gutsche, C Hanhart, C Lourenço, A Masoni, M Mikhasenko, R Mitchell, C Patrignani, C Schwanda, et al. Review of particle physics. *Physical Review D*, 110(3), 2024.
- [2] Claudia Patrignani, P Richardson, OV Zenin, R-Y Zhu, A Vogt, S Pagan Griso, L Garren, DE Groom, M Karliner, DM Asner, et al. Review of particle physics, 2016-2017. *Chin. Phys. C*, 40:100001, 2016.
- [3] Juerg Beringer, J-F Arguin, RM Barnett, K Copic, O Dahl, DE Groom, C-J Lin, J Lys, H Murayama, CG Wohl, et al. Review of particle physics. *Physical Review D—Particles, Fields, Gravitation, and Cosmology*, 86(1):010001, 2012.
- [4] E Eichten, K Gottfried, T Kinoshita, KD Lane, and T-M Yan. Charmonium: the model. *Physical Review D*, 17(11):3090–3117, 1978.
- [5] Estia Eichten, K Gottfried, T Kinoshita, KD Lane, and Tung-Mow Yan. Charmonium: comparison with experiment. *Physical review D*, 21(1):203, 1980.
- [6] Stephen Godfrey and Nathan Isgur. Mesons in a relativized quark model with chromodynamics. *Physical Review D*, 32(1):189, 1985.
- [7] Estia J Eichten and Chris Quigg. Mesons with beauty and charm: Spectroscopy. *Physical Review D*, 49(11):5845, 1994.
- [8] T Barnes, Stephen Godfrey, and ES Swanson. Higher charmonia. *Physical Review D—Particles, Fields, Gravitation, and Cosmology*, 72(5):054026, 2005.
- [9] Wei-Jun Deng, Hui Liu, Long-Cheng Gui, and Xian-Hui Zhong. Charmonium spectrum and electromagnetic transitions with higher multipole contributions. *Physical Review D*, 95(3):034026, 2017.
- [10] Krishna Kingkar Pathak, Satyadeep Bhattacharya, and Tapashi Das. Parameterisation space for cornell potential in a qcd potential model. *The European Physical Journal C*, 82(11):1081, 2022.
- [11] M Sreelakshmi and Akhilesh Ranjan. Mass spectroscopy of charmonium using cornell plus exponential potential. In *Proceedings of the DAE-BRNS symposium on nuclear physics. V. 66*, pages 2–2, 2022.
- [12] Zaki Ahmad, Ishrat Asghar, Bilal Masud, and M Atif Sultan. Charmonium spectrum and its decay properties. *The European Physical Journal A*, 61(9):200, 2025.
- [13] Tarik Akan. Predicting $b\bar{c}$ meson mass spectra using neural network with combined cornell and quadratic potentials. *Süleyman Demirel Üniversitesi Fen Bilimleri Enstitüsü Dergisi*, 29(2):426–433, 2025.
- [14] Akhilesh Ranjan et al. Mass spectroscopy of charmonium using a screened potential. *International Journal of Theoretical Physics*, 64(3):1–12, 2025.
- [15] Frithjof Karsch, MT Mehr, and Helmut Satz. Color screening and deconfinement for bound states of heavy quarks. *Zeitschrift für Physik C Particles and Fields*, 37(4):617–622, 1988.
- [16] Sanatan Digal, Peter Petreczky, and Helmut Satz. Quarkonium feed-down and sequential suppression. *Physical Review D*, 64(9):094015, 2001.

- [17] Timofey Solomko. Cornell potential from soft wall holographic approach to qcd. *Acta Physica Polonica B, Proceedings Supplement*, 16(8):A3, 2023.
- [18] Benoît Assi and Michael L Wagman. Baryons, multihadron systems, and composite dark matter in nonrelativistic qcd. *Physical Review D*, 108(9):096004, 2023.
- [19] Benoît Assi and Michael L Wagman. Tetraquarks made of sufficiently unequal-mass heavy quarks are bound in qcd. *Physical Review D*, 110(9):094001, 2024.
- [20] Sandro Sorella. Green function monte carlo with stochastic reconfiguration. *Physical review letters*, 80(20):4558, 1998.
- [21] Giuseppe Carleo and Matthias Troyer. Solving the quantum many-body problem with artificial neural networks. *Science*, 355(6325):602–606, 2017.
- [22] Halil Mutuk. Cornell potential: a neural network approach. *Advances in High Energy Physics*, 2019(1):3105373, 2019.
- [23] Hakan Ciftci, Richard L Hall, and Nasser Saad. Asymptotic iteration method for eigenvalue problems. *Journal of Physics A: Mathematical and General*, 36(47):11807–11816, 2003.
- [24] Ramesh Kumar and Fakir Chand. Asymptotic study to the n-dimensional radial schrödinger equation for the quark-antiquark system. *Communications in Theoretical Physics*, 59(5):528–532, 2013.
- [25] Antony Prakash Monteiro, Manjunath Bhat, and KB Vijaya Kumar. $c\bar{b}$ spectrum and decay properties with coupled channel effects. *Physical Review D*, 95(5):054016, 2017.
- [26] Tarik Akan. Spin-averaged B_c spectrum in a cornell-type potential using vmc baseline and gfm evolution. *arXiv preprint arXiv:2511.10986*, 2025.